NANOSYSTEMS:
PHYSICS, CHEMISTRY, MATHEMATICS

Aljunid S.Z.Z., et al. *Nanosystems: Phys. Chem. Math.*, 2024, **15** (2), 184–191.
http://nanojournal.ifmo.ru
DOI 10.17586/2220-8054-2024-15-2-184-191

Original article

Q-switched and mode-locked pulse generations with Ti_3AlC_2 absorber

Syed Ziad Z. Aljunid[1], Nurul Athirah M. A. Ghafar[1], Bilal A. Ahmad[2], Retna Apsari[3], Sulaiman W. Harun[1,3]

[1]Department of Electrical Engineering, Faculty of Engineering, University of Malaya, Kuala Lumpur 50603, Malaysia

[2]Department of Communication Engineering, Al-Ma'moon University College, Al-Washash, 700921 Baghdad, Iraq

[3]Department of Physics, Faculty of Science and Technology, Airlangga University, Surabaya 60115 Indonesia

Corresponding author: Sulaiman W. Harun, swharun@um.edu.my

ABSTRACT Exploring advanced saturable absorber (SA) materials that exhibit exceptional performance for achieving Q-switching and mode-locking operations remains a vibrant area of research in the field of fiber lasers. The remarkable optical nonlinearity, coupled with high thermal and chemical stability of MAX phase materials, positions them as promising candidates for high-performance SAs. In this study, we demonstrated the potential of Ti_3AlC_2 MAX phase as an effective material for Q-switched and mode-locked fiber laser applications. The Ti_3AlC_2 film was synthesized through a straightforward and cost-effective casting method employing polyvinyl alcohol (PVA) as a host material. The SA was cleverly constructed from the film, utilizing a sandwich-structured fiber-ferrule platform, and seamlessly integrated into an Erbium-doped fiber laser (EDFL) ring cavity. Initially, a stable Q-switched laser was realized at a center wavelength of 1531 nm. The repetition rate exhibited a commendable increase from 35.0 to 50.8 kHz, and the pulse width reduced from 6.58 to 3.40 μs as the pump power was adjusted within the range of 25.98 to 58.29 mW. Notably, the maximum output power of 2.49 mW and a pulse energy of 49.02 nJ were recorded at a pump power of 58.29 mW. Subsequently, an additional 200 m long single-mode fiber was added into a similar laser cavity, leading to the generation of a stable mode-locked laser at a threshold pump power of 81.37 mW, operating at a central wavelength of 1558.96 nm. The observed stable repetition rate of 969.3 kHz, coupled with a pulse duration of 300 ns, demonstrated robust performance as the pump power increased from 81.37 to 113.68 mW. These findings highlight the exceptional performance of Ti_3AlC_2 SA for both Q-switching and mode-locking applications. The versatility of these lasers makes them valuable for diverse applications, including micromachining of materials, frequency comb generation, and remote sensing.

KEYWORDS Ti_3AlC_2, max phase material, Q-switching, mode-locking, saturable absorber, erbium-doped fiber laser

FOR CITATION Aljunid S.Z.Z., Ghafar N.A.M.A., Ahmad B.A., Apsari R., Harun S.W. Q-switched and mode-locked pulse generations with Ti_3AlC_2 absorber. *Nanosystems: Phys. Chem. Math.*, 2024, **15** (2), 184–191.

1. Introduction

Fiber lasers, as exemplary representatives of third-generation laser technology, have emerged as highly promising tools across numerous scientific and industrial domains, commanding a substantial share of the commercial laser market [1]. These versatile lasers can be categorized into two primary operational modes: continuous and pulsed. Pulsed fiber lasers, characterized by high pulse energy and short pulse widths, have significantly broadened their applications in fiber optic communication, automotive manufacturing, laser cutting, medical devices, and various other sectors [2]. Pulsed lasers can be achieved through two main techniques: Q-switching and mode-locking, with options for both active and passive implementation. In recent years, passive techniques have garnered increased attention due to their inherent advantages in terms of simplicity, flexibility, compactness, and cost-effectiveness. Unlike their active counterparts, passive pulsed lasers do not rely on unwieldy and intricate optical modulators or complex electronic drivers. Instead, they can generate laser pulses by merely incorporating a saturable absorber (SA) within the resonant cavity. The SA, a pivotal component in passive Q-switched and mode-locked lasers, assumes a crucial role in shaping the laser output [3].

The evolution of passive pulsed lasers is intrinsically tied to advancements in SA materials. To date, several emerging nanomaterials have displayed promising saturable absorption properties suitable for practical saturable absorbers (SAs) [4]. Despite the prevalent use of III–V compound semiconductors in commercially available ultrafast lasers [5], intensive investigations have been conducted on a diverse range of nanomaterials to assess their saturable absorption potential. These materials encompass carbon nanotubes (CNTs) [6], graphene [7], topological semimetals [8], topological

insulators (TIs) [9], black phosphorus (BPs) [10], transition metal dichalcogenides (TMDCs) [11], gold nanoparticles [12], and MXenes [13].

Among the nano-materials mentioned, MXenes stand out as a new family of 2D materials. Their exceptional electronic and photonic properties [14] have thrust them into the limelight within the realms of materials science and engineering. MXenes are characterized by the general formula $M_{n+1}X_nT_x$ (where n ranges from 1 to 3, M represents an early transition metal, X signifies carbon and/or nitrogen, and T denotes surface terminations). These remarkable materials are derived from their ternary MAX phase precursors through a process of chemical etching [15]. Despite their extensive applicability in diverse fields, such as electrochemical capacitors, water purification, chemical catalysts, and biosensors [16, 17], the use of a chemical etching method involving hydrofluoric (HF) acid presents a significant hurdle to their large-scale production due to the severe toxicity associated with HF acid.

As a result, there has been a significant surge in technical interest in precursor materials known as MAX phases. These MAX phases still exhibit notable photonic and electronic properties that are comparable to those of MXenes, further fueling research in this area [18]. MAX phases constitute a category of ductile ceramic materials with the chemical formula $M_{n+1}AX_n$ (where $n = 1, 2, 3\ldots$), with M representing an early transition metal, A corresponding to the IIIA or IVA group element, and X signifying either nitrogen or carbon. These MAX phases are renowned for their resilience and find application in fields such as nuclear engineering, high-temperature applications, and aerospace due to their robust nature [15, 19]. In this work, we propose a novel Q-switched and mode-locked fiber laser by incorporating Ti_3AlC_2 PVA film in the Erbium-doped fiber laser (EDFL) cavity. The SA film was fabricated by using embedding Ti_3AlC_2 powder in PVA as a host polymer to form a absorb film. The SA film has saturable absorption and saturation intensity of 2 % and 1000 MW/cm^2, respectively.

2. Fabrication and characterization of Ti_3AlC_2/PVA-based SA

Ti_3AlC_2 powder, characterized by its 99.9 % purity and sourced from Carbon-Ukraine Ltd, was used in this work to fabricate a composite thin film through integration into a polyvinyl alcohol (PVA) solution. The PVA solution preparation involved dissolving 1 g of the compound in 120 ml of distilled water. This mixture underwent stirring in a vessel for approximately 24 hours at a speed of 300 rpm and a temperature of 200 °C, ensuring complete dissolution of the material. Subsequently, 40 ml of the prepared PVA solution was transferred to a separate beaker, where it served as the base for the composite solution. Here, 10 mg of Ti_3AlC_2 powder was added, initiating a stirring process lasting 24 hours. Following this, the solution underwent sonication in an ultrasonic bath for an additional 3 hours, resulting in the formation of a homogeneous composite Ti_3AlC_2 PVA solution. To complete the fabrication process, a small quantity of the solution was directly poured onto a petri dish, allowing it to spread naturally. The solution-laden petri dish was left undisturbed for approximately 48 hours, enabling the formation and drying of the composite film. Subsequently, the film was delicately peeled off and strategically positioned between two FC/PC fiber ferrules via a fiber adaptor. This meticulous arrangement yielded a saturable absorber (SA) device with an insertion loss measuring approximately 2.4 dB. A comprehensive visualization of the step-by-step procedure for fabricating the SA thin film is illustrated in Fig. 1.

FIG. 1. Illustration of Ti_3AlC_2 PVA film preparation

The material characteristics of the Ti_3AlC_2 film were thoroughly investigated through field-emission scanning electron microscopy (FESEM) and energy-dispersive X-ray spectroscopy (EDX). Fig. 2(a) presents the FESEM image, revealing an even dispersion of Ti_3AlC_2 particles within the PVA matrix. Subsequently, the EDX spectrum of the Ti_3AlC_2 film, illustrated in Fig. 2(b), exhibits prominent peaks corresponding to titanium (Ti), aluminum (Al), carbon (C), and oxygen (O). Quantitative analysis confirms the presence of 72.8 wt.% Ti, 10.4 wt.% Al, 9.5 wt.% C, and 7 wt.% O in the composite. Moving forward, the nonlinear transmission curve of the Ti_3AlC_2 PVA thin film was determined using a twin-balance detection method. A home-built mode-locked Erbium-doped fiber laser (EDFL) operating at 1558 nm, with a temporal width of 3.62 ps and a repetition rate of 1.9 MHz, served as the input light source. Fig. 2(c) depicts the

measured nonlinear transmission output intensity plotted against the peak intensity of the incident light, accompanied by a fitted curve described by the equation [20]:

$$T(I) = 1 - \Delta T \cdot \exp\left(\frac{-I}{I_{sat}}\right) - T_{ns}.$$

Here (I) represents the transmitted intensity, ΔT is the saturable absorption, I is the input pulse intensity, T_{ns} is the non-saturable absorption, and I_{sat} is the saturation intensity. The measured saturable absorption, non-saturable absorption, and saturation intensity were found to be approximately 2 %, 59 %, and 1000 MW/cm^2, respectively.

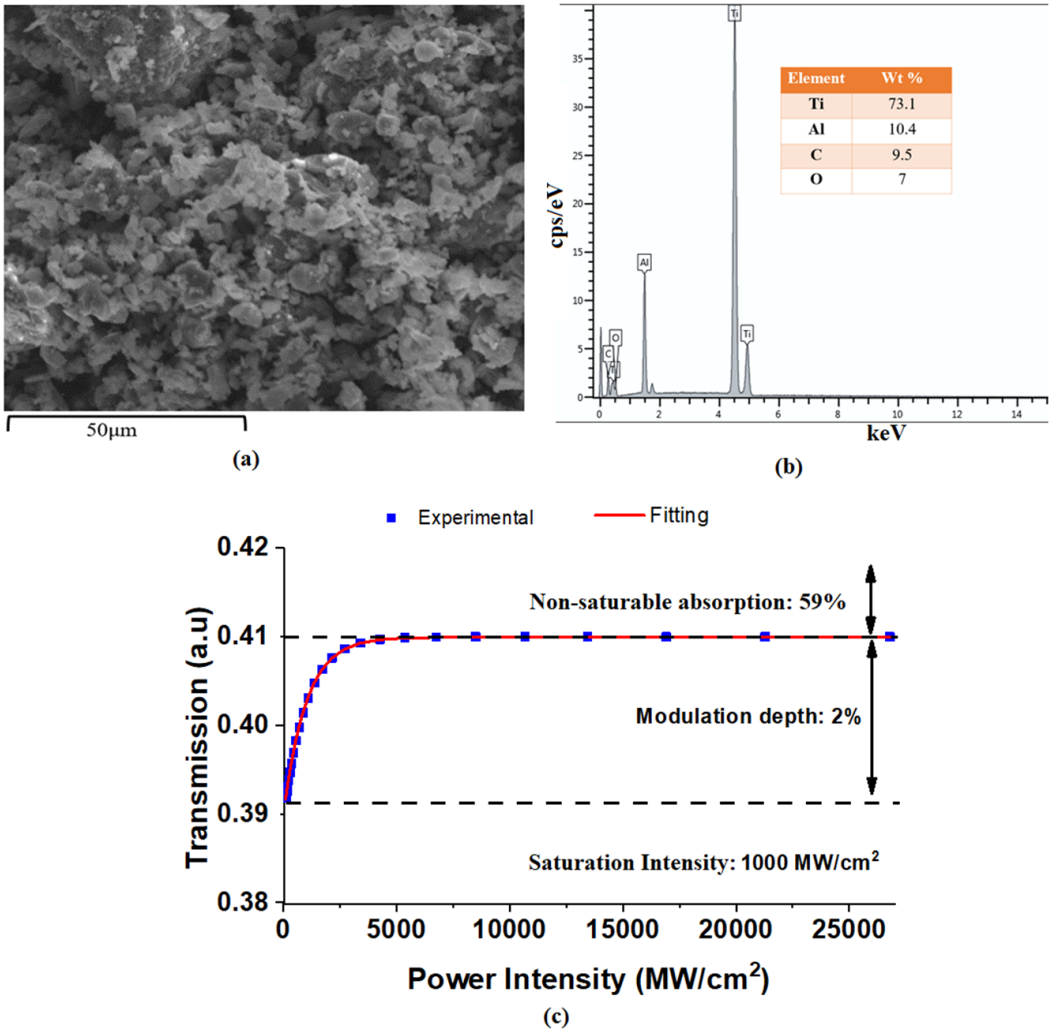

FIG. 2. The Ti_3AlC_2 PVA film characteristics (a) FESEM image (b) EDX analysis result (c) nonlinear transmission curve

3. Laser configuration

The Q-switched laser setup was firstly constructed, leveraging an all-fiber EDFL ring structure, as depicted in Fig. 3. In this configuration, an Erbium-doped fiber (EDF) served as the active medium, while the previously fabricated Ti_3AlC_2-PVA thin film functioned as the SA. The inset figure provides an actual image of the fabricated Ti_3AlC_2-PVA thin film, featuring a thickness of approximately 50 μm. The EDF used has a length of 1.8 m, a numerical aperture (NA) of 0.23, and core/cladding diameters of 4 μm/125 μm, with a peak absorption of 23 dB/m at the pumping wavelength. A 980 nm laser diode, facilitated by a 980/1550 nm wavelength-division multiplexer (WDM), co-pumped the EDF. To ensure unidirectional propagation, a polarization-insensitive optical isolator was incorporated into the cavity resonator. For both temporal and spectral diagnostics, a 20/80 fused-fiber coupler was employed to tap out the output laser.

The Ti_3AlC_2 SA played a key role in modulating the intra-cavity loss to produce a Q-switched pulse train. It also facilitates the phase-locking of longitudinal modes within the EDFL ring cavity to produce mode-locked pulses. The fused-fiber coupler allocated 20 % of the oscillating laser for output, while retaining the remaining 80 % within the cavity for sustained operation. To investigate the laser performance, a comprehensive measurement setup was implemented. A

digital oscilloscope and a radio frequency spectrum analyzer (RFSA) were utilized for assessing optical parameters in the time and frequency domains, respectively. These measurements were conducted in tandem with a fast photodiode (PD). Simultaneously, an optical spectrum analyzer (OSA) with a high resolution of 0.02 nm was deployed to examine the laser's spectral characteristics. Additionally, the average output power was precisely gauged using an optical power meter coupled with an InGaAs detector.

The laser cavity underwent a strategic modification to allow mode-locked pulse generation by introducing a 200 m long single-mode fiber (SMF) between the SA device and the output coupler. This additional SMF served the dual purpose of managing the dispersion regime and enhancing nonlinearity within the system. Consequently, the total length of the mode-locked laser cavity extended to approximately $\sim$ 206 m. The modified cavity comprised a 1.8 m long EDF, a 0.7 m long WDM fiber, and the newly incorporated 203.5 m long SMF. Each segment possessed distinct group velocity dispersion (GVD) values: approximately 27.6 ps^2/km for the EDF, -48.5 ps^2/km for the WDM fiber, and -21.7 ps^2/km for the SMF. The summation of these dispersion values resulted in an estimated total cavity dispersion of approximately -4.4 ps^2. This modification strategically managed the dispersion characteristics of the laser cavity, contributing to the optimization of mode-locked pulse generation.

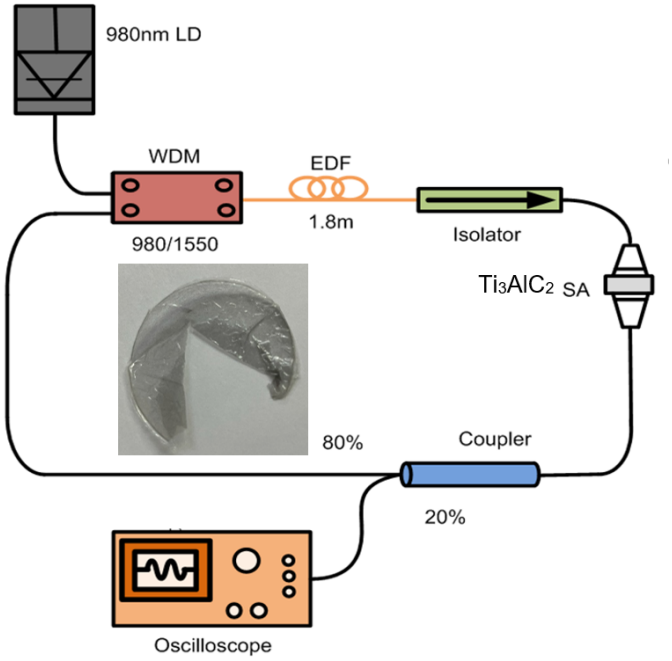

FIG. 3. Configuration of the proposed EDFL with Ti_3AlC_2 SA. Inset shows a real image of the Ti_3AlC_2 PVA film. The mode-locking was realized by adding 200 m long SMF in between the SA and output coupler.

4. Result and discussion

To eliminate the possibility of self-Q-switching or self-mode-locking operations in the EDFL without the Ti_3AlC_2 SA, initial experiments were conducted without inserting the SA into the laser cavity. During this phase, only continuous-wave (CW) operation was observed while adjusting the pump power. However, upon the introduction of the Ti_3AlC_2 SA into the laser cavity, self-started passively Q-switched pulse trains were observed when the pump power exceeded 26.0 mW. Fig. 4(a) provides a comparison of the output spectrum of the laser in CW and Q-switched operations, obtained without and with the SA at the threshold pump power of 26.0 mW. Notably, the peak laser wavelength experienced a blue shift, transitioning from 1567 to 1531 nm after the integration of the Ti_3AlC_2 SA into the cavity. This blue-shifted wavelength is a result of increased loss within the cavity, prompting the laser to emit at shorter wavelength region to achieve higher amplification gain and compensate for additional losses. The Q-switched laser exhibited a 3 dB spectral bandwidth of 2.5 nm, notably broader than the CW laser, which had a bandwidth of 0.5 nm. This spectral broadening can be attributed to the self-phase modulation effect within the laser cavity. The Q-switching operation was sustained up to a pump power of 58.3 mW, showing the effectiveness and stability of the Ti_3AlC_2 SA in inducing and maintaining Q-switched pulses.

The oscilloscope trace of the Q-switched pulse train under maximum pump power is illustrated in Fig. 4(b), revealing a highly consistent Q-switching operation. Inset of Fig. 4(b) depicts the temporal profile of two adjacent pulses, demonstrates a pulse width of 3.4 μs and a pulse interval of 19.4 μs between the Q-switched pulses. This pulse interval

corresponds to a pulse repetition rate of 50.80 kHz. The stability of the pulsing is then assessed through the measurement of the radio frequency (RF) spectrum, as depicted in Fig. 4(c). The RF spectrum of the Q-switched pulse exhibits excellent stability, with a signal-to-noise ratio (SNR) of approximately 71.4 dB achieved at the fundamental frequency of 50.80 kHz. It is noteworthy that the characteristics of the pulse trains and the optical spectrum remain largely unchanged when varying the polarization state in the cavity. This observation indicates that the Q-switching operation of the fiber laser is polarization insensitive, further enhancing its practical utility and stability.

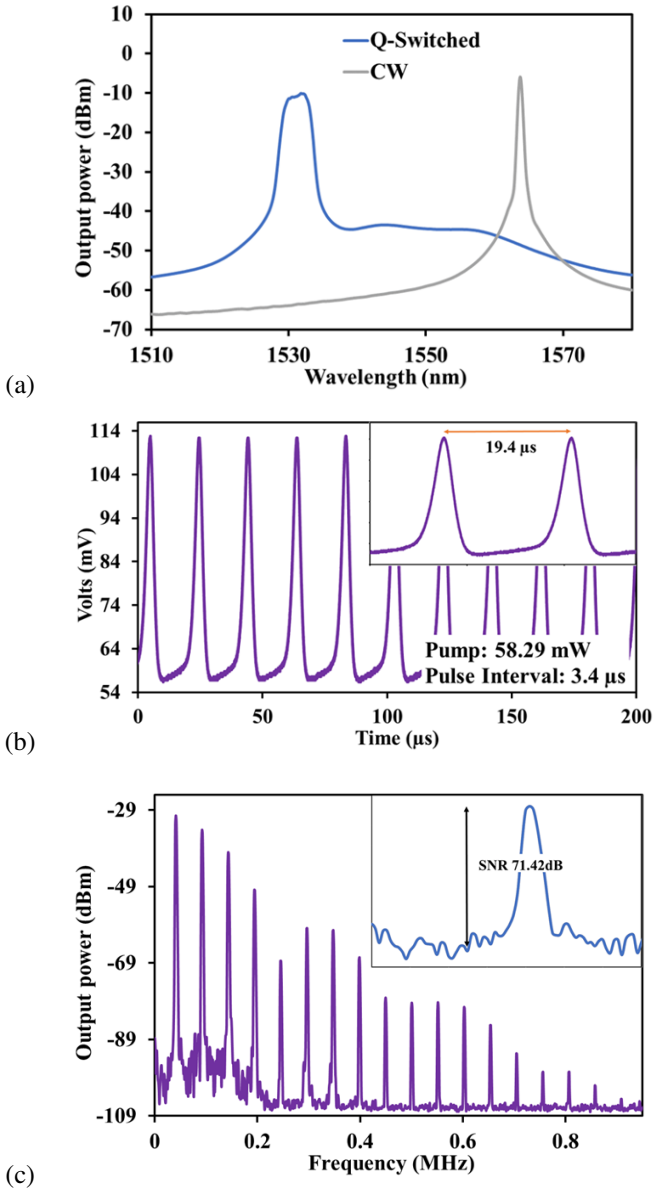

FIG. 4. Q-switching performances (a) Output spectrum of the EDFL with and without Ti_3AlC_2 SA at 26.0 mW pump, (b) typical oscilloscope pulse train at 58.3 mW. Inset shows the temporal profile of two adjacent pulses, and (c) RF spectrum at the pump power of 58.3 mW.

The characteristics of the laser pulses in relation to pump power are illustrated in Fig. 5. Fig. 5(a) presents the dependence of the pulse repetition rate and pulse width on the pump power. Unlike mode-locking operations, the generation of Q-switched pulses relies on the saturation of the SA, causing the repetition rate to be influenced by pump power rather than cavity length. As the pump power increased from 26.0 to 58.3 mW, the repetition rate displayed an almost linear growth, ranging from 35.0 to 50.8 kHz. This behavior stems from the faster saturation of the SA with increasing pump power, leading to a corresponding increase in the repetition rate. Simultaneously, the pulse width decreased from 6.58 to 3.40 μs with the escalating pump power. Both the trends in repetition rate and pulse width align with the typical characteristics of Q-switched fiber lasers. In Fig. 5(b), the average output power and pulse energy characteristics are plotted against pump power. With pump power increasing from 26.0 to 58.3 mW, the average output power exhibited nearly linear growth,

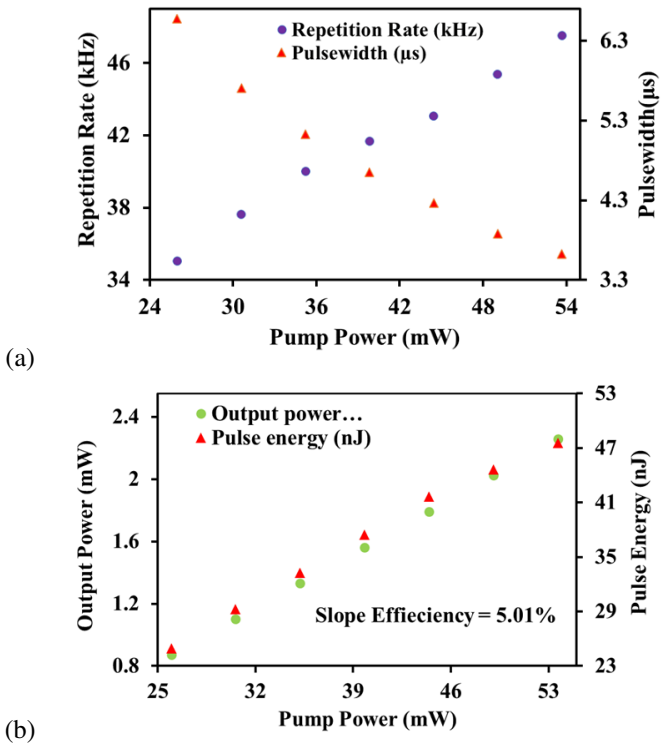

FIG. 5. The variation of (a) repetition rate and pulse width (b) output power and pulse energy as the pump power increases

ranging from 0.87 to 2.49 mW. The slope efficiency, calculated from this relationship, is approximately 5.0 %. The single pulse energy reached up to 49.0 nJ, highlighting the effectiveness of the SA in generating Q-switched pulses.

Subsequently, the introduction of an additional 200 m length of SMF into the existing cavity aimed to balance the dispersion and nonlinearity, facilitating the initiation of self-started mode-locked pulses. The EDFL initiated the generation of mode-locked pulses at a threshold pump power of 81.37 mW. The mode-locking operation continued as the pump power was further increased, sustaining up to 113.68 mW. This indicates that the use of the Ti_3AlC_2 SA was effectively facilitating pulse shaping and stabilizing the mode-locked generation within the EDFL cavity. Fig. 6(a) illustrates the output spectrum of the mode-locked EDFL at a pump power of 81.37 mW. The laser operated at a wavelength of 1558.96 nm, a shift from the previous Q-switched laser's wavelength due to the significantly higher pumping power employed in the mode-locked operation.

In Fig. 6(b), a typical oscilloscope trace of the mode-locked pulse train at a pump power of 113.68 mW is presented, showing highly stable pulses with a uniform distribution of peak intensity. The inset of Fig. 6(b) displays the corresponding two-pulse envelopes with a time interval of 1.03 ns, aligning well with the round-trip time of the cavity. Notably, no pulse shivering was observed in the oscilloscope trace. The mode-locked laser operates at a pulse rate of 969.3 kHz and a pulse duration of 300 ns. Fig. 6(c) illustrates the radio frequency (RF) spectrum with a bandwidth of 15 MHz, providing a visual representation of the stability of the mode-locked laser with a fundamental repetition rate of 969.3 kHz. The signal-to-noise ratio (SNR) of the fundamental frequency was measured at 75.16 dB, further attesting to the stability of the mode-locked pulses.

In Fig. 6(d), the graph of output power and pulse energy as a function of pump power is presented, revealing a linear relationship between both parameters and pump power. The maximum average output power reached 3.19 mW, corresponding to a pulse energy of 3.29 nJ under a pump power of 113.68 mW. A continuous 4-hour observation of the oscilloscope traces and optical spectra of the mode-locked pulses verified the long-term stability of the fiber laser. The pulse train and the central wavelength of the spectrum remained consistently stable throughout the observation period. Additionally, after a 24-hour pause in laser operation followed by restarting the pump, the mode-locked pulses continued to output stably, and the laser center wavelength remained stable at 1558.96 nm, highlighting the long-term stability of the laser system.

In addition to its applications in Q-switching and mode-locking, Ti_3AlC_2 material shows promising potential in random lasing applications [21]. By leveraging its unique properties, Ti_3AlC_2 can be utilized to create disordered structures, exploiting phenomena like multiple light scattering to facilitate the development of the innovative low threshold random lasers [22].

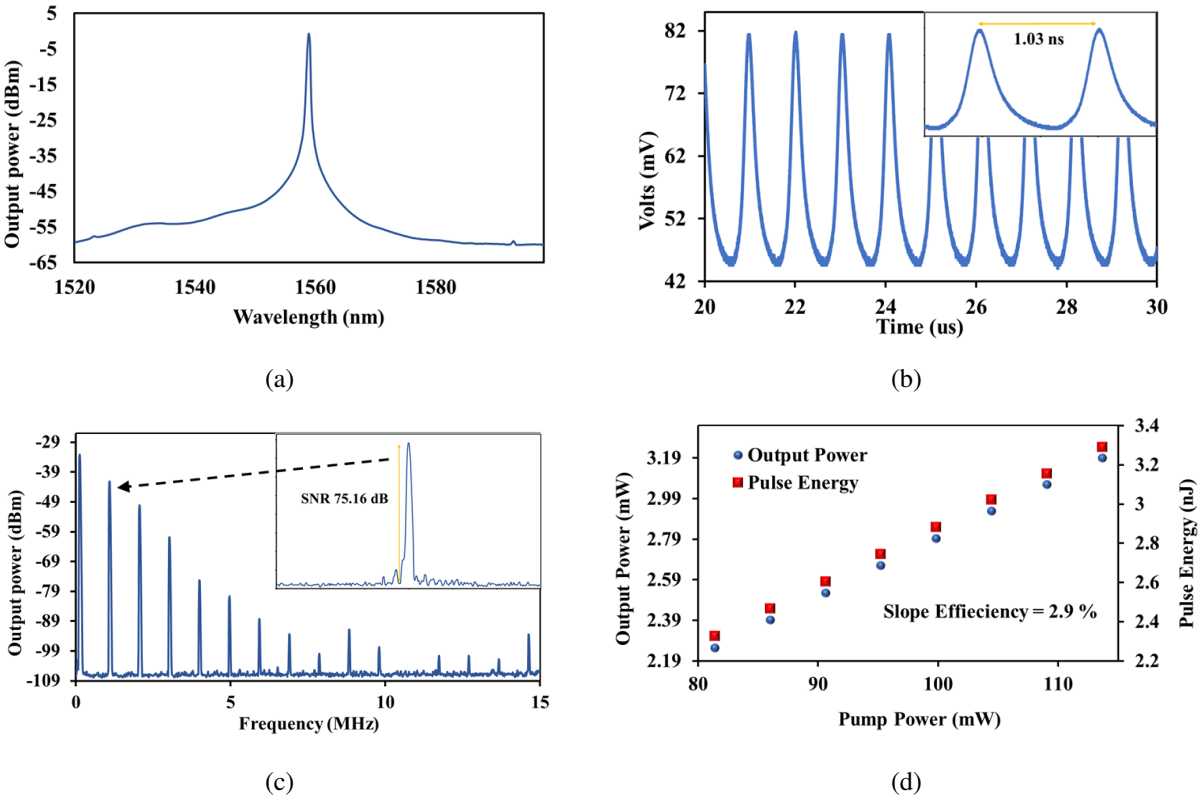

FIG. 6. Mode-locking performance: (a) output spectrum (b) Oscilloscope trace. Inset shows the two-pulse envelop (c) RF spectrum. Inset shows the enlarged fundamental mode (d). Output power and pulse energy versus pump power.

5. Conclusion

The successful demonstration of both Q-switched and mode-locked EDFLs operating in the 1.55 μm regime, utilizing the newly developed Ti_3AlC_2 as a SA, marks a significant achievement in fiber laser technology. Initially, the Ti_3AlC_2 thin film was introduced into the laser cavity, sandwiched between two fiber ferrules, to generate a passively Q-switched EDFL. The resulting stable Q-switched pulse train operated at a center wavelength of 1531 nm. As the pump power increased from 25.98 to 58.29 mW, the repetition rate rose from 35.0 to 50.8 kHz, while the pulse width decreased from 6.58 to 3.40 μs. At a pump power of 58.29 mW, the system achieved a maximum output power of 2.49 mW and a pulse energy of 49.02 nJ. The Q-switched EDFL exhibited a high SNR of 71.42 dB, indicating stable pulse generation. The introduction of a 200 m SMF into the laser cavity allowed for the transition to a mode-locking regime, resulting in a laser with a central wavelength of 1558.96 nm. In this mode-locked laser configuration, the repetition rate reached 969.3 kHz, and the pulse width measured 300 ns within the pump power range of 81.37 to 113.68 mW. These results indicates the potential of the Ti_3AlC_2-based SA as a promising candidate for both Q-switching and mode-locking applications in EDFLs.

References

[1] Dong L., Samson B. *Fiber Lasers: Basics, Technology, and Applications*. CRC press, New York, 2016.
[2] Shi W., et al. Fiber lasers and their applications. *Applied optics*, 2014, **53** (28), P. 6554–6568.
[3] Sun S., et al. Demonstration of passively Q-switched and mode-locked operations through dispersion control in Er-doped fiber lasers with a cylindrite-based saturable absorber. *J. of Luminescence*, 2022, **250**, 119064.
[4] Liu W., et al. 2D Materials for Fiber Lasers: Recent Advances of 2D Materials in Nonlinear Photonics and Fiber Lasers. *Advanced Optical Materials*, 2020, **8** (8), 2070031.
[5] Zhang Y., et al. Study of the influence of SESAM parameters on the evolution of mode-locked pulses at different repetition rates. *Applied Physics B*, 2021, **127** (8), P. 1–10.
[6] Nishizawa N., et al. Dynamics of a dispersion-managed passively mode-locked Er-doped fiber laser using single wall carbon nanotubes. *Photonics*, 2015, **2** (3), P. 808–824.
[7] Haris H., et al. Generation of Vector Soliton Pulses with Graphene Oxide Film in Mode-locked Erbium-doped Fiber Laser Cavity. *Nonlinear Optics Quantum Optics-Concepts in Modern Optics*, 2020, **52** (1–2), P. 111–118.
[8] Hu J.-W., et al. Passively mode-locked Er-doped fiber laser based on a semi-metallic InBi saturable absorber. *J. of Physics D: Applied Physics*, 2021, **55** (10), 105104.
[9] Haris H., et al. Mode-Locked YDFL Using Topological Insulator Bismuth Selenide Nanosheets as the Saturable Absorber. *Crystals*, 2022, **12** (4), 489.

[10] Ismail E., et al. Black phosphorus crystal as a saturable absorber for both a Q-switched and mode-locked erbium-doped fiber laser. *RSC Advances*, 2016, **6** (76), P. 72692–72697.
[11] Tiu Z., et al. Application of transition metal dichalcogenide in pulsed fiber laser system. *Materials Research Express*, 2019, **6** (8), 082004.
[12] Rosol A.H.A., et al. Nanosecond pulses generation with rose gold nanoparticles saturable absorber. *Indian J. of Physics*, 2020, **94** (7), P. 1079–1083.
[13] Jafry A.A.A., et al. MXene $Ti_3C_2T_x$ as a passive Q-switcher for erbium-doped fiber laser. *Optical Fiber Technology*, 2020, **58**, 102289.
[14] Fu B., et al. MXenes: Synthesis, optical properties, and applications in ultrafast photonics. *Small*, 2021, **17** (11), 2006054.
[15] Gonzalez-Julian J. Processing of MAX phases: From synthesis to applications. *J. of the American Ceramic Society*, 2021, **104** (2), P. 659–690.
[16] Khazaei M., et al. Recent advances in MXenes: From fundamentals to applications. *Current Opinion in Solid State and Materials Science*, 2019, **23** (3), P. 164–178.
[17] Gogotsi Y., Anasori B. The rise of MXenes. *ACS Nano*, 2019, **13** (8), P. 8491–8494.
[18] Zhang Z., et al. On the formation mechanisms and properties of MAX phases: A review. *J. of the European Ceramic Society*, 2021, **41** (7), P. 3851–3878.
[19] Sun Z. Progress in research and development on MAX phases: a family of layered ternary compounds. *Int. Materials Reviews*, 2011, **56** (3), P. 143–166.
[20] Wu K., et al. High-performance mode-locked and Q-switched fiber lasers based on novel 2D materials of topological insulators, transition metal dichalcogenides and black phosphorus: review and perspective. *Optics Communications*, 2018, **406**, P. 214–229.
[21] Bazhenov A.Y., et al. Random Laser Based on Materials in the Form of Complex Network Structures. *JETP Letters*, 2023, **117** (11), P. 814–820.
[22] Wiersma D.S. Disordered photonics. *Nature Photonics*, 2013, **7** (3), P. 188–196.

Submitted 6 January 2024; revised 25 March 2024; accepted 26 March 2024

Information about the authors:

Syed Ziad Z. Aljunid – Department of Electrical Engineering, Faculty of Engineering, University of Malaya, Kuala Lumpur 50603, Malaysia; ORCID 0009-0003-9890-6926; 22064743@siswa.um.edu.my

Nurul Athirah M. A. Ghafar – Department of Electrical Engineering, Faculty of Engineering, University of Malaya, Kuala Lumpur 50603, Malaysia; ORCID 0000-0003-4557-5695; athirahghafar97@gmail.com

Bilal A. Ahmad – Department of Communication Engineering, Al-Ma'moon University College, Al-Washash, 700921 Baghdad, Iraq; belalanwer@yahoo.com

Retna Apsari – Department of Physics, Faculty of Science and Technology, Airlangga University, Surabaya (60115) Indonesia; ORCID 0000-0002-3597-5938; retna-a@fst.unair.ac.id

Sulaiman W. Harun – Department of Electrical Engineering, Faculty of Engineering, University of Malaya, Kuala Lumpur 50603, Malaysia; Department of Physics, Faculty of Science and Technology, Airlangga University, Surabaya (60115) Indonesia; ORCID 0000-0003-4879-5853; swharun@um.edu.my

Conflict of interest: the authors declare no conflict of interest.